Atmospheric
Chemistry
and Physics
Discussions

Open Access

EGU

1 **Predicting the glass transition temperature and viscosity of secondary**

2 **organic material using molecular composition**

3

4

5 **Wing-Sy Wong DeRieux[1][§], Ying Li[1][§], Peng Lin[2], Julia Laskin[2], Alexander Laskin[2],**

6 **Allan K. Bertram[3], Sergey A. Nizkorodov[1], and Manabu Shiraiwa[1][*]**

7

8 [1] Department of Chemistry, University of California, Irvine, CA 92697-2025, USA

9 [2] Department of Chemistry, Purdue University, West Lafayette, IN 47907-2084, USA

10 [3] Department of Chemistry, University of British Columbia, Vancouver, BC V6T 1Z1, Canada

11

12 [§] These authors contributed equally to this work.

13 [*] Correspondence to: M. Shiraiwa (m.shiraiwa@uci.edu)

14

Atmospheric
Chemistry
and Physics
Discussions

15 **Abstract:**

16 Secondary organic aerosols (SOA) account for a large fraction of submicron particles in the

17 atmosphere. SOA can occur in amorphous solid or semi-solid phase states depending on

18 chemical composition, relative humidity (RH), and temperature. The phase transition between

19 amorphous solid and semi-solid states occurs at the glass transition temperature (T_g). We have

20 recently developed a method to estimate T_g of pure compounds containing carbon, hydrogen, and

21 oxygen atoms (CHO compounds) with molar mass less than 450 g mol^{-1} based on their molar

22 mass and atomic O:C ratio. In this study, we refine and extend this method for CH and CHO

23 compounds with molar mass up to ~1100 g mol^{-1} using the number of carbon, hydrogen, and

24 oxygen atoms. We predict viscosity from the T_g-scaled Arrhenius plot of fragility (viscosity vs.

25 T_g/T) as a function of the fragility parameter D. We compiled D values of organic compounds

26 from literature, and found that D approaches a lower limit of ~10 (+/- 1.7) as the molar mass

27 increases. We estimated viscosity of α-pinene and isoprene SOA as a function of RH by

28 accounting for hygroscopic growth of SOA and applying the Gordon-Taylor mixing rule,

29 reproducing previously published experimental measurements very well. Sensitivity studies were

30 conducted to evaluate impacts of T_g, D, hygroscopicity parameter (κ), and the Gordon-Taylor

31 constant on viscosity predictions. Viscosity of toluene SOA was predicted using the elemental

32 composition obtained by high-resolution mass spectrometry (HRMS), resulting in a good

33 agreement with the measured viscosity. We also estimated viscosity of biomass burning particles

34 using the chemical composition measured by HRMS with two different ionization techniques:

35 electrospray ionization (ESI) and atmospheric pressure photoionization (APPI). Due to

36 differences in detected organic compounds and signal intensity, predicted viscosities at low RH

37 based on ESI and APPI measurements differ by 2-5 orders of magnitude. Complementary

Atmospheric
Chemistry
and Physics
Discussions

38   measurements of viscosity and chemical composition are desired to further constrain RH-

39   dependent viscosity in future studies.

40

41   **1. Introduction**

42   Secondary organic aerosols (SOA) account for a large fraction of submicron particles in the

43   atmosphere and they play an important role in climate, air quality and public health (Goldstein

44   and Galbally, 2007; Jimenez et al., 2009). Traditionally, SOA particles were assumed to be

45   liquid with dynamic viscosity η below 10^2 Pa s, but a number of recent studies have shown that

46   they can also adopt amorphous semi-solid ($10^2 \leq \eta \leq 10^{12}$ Pa s), or glassy solid ($\eta > 10^{12}$ Pa s)

47   states, depending on chemical composition, relative humidity (RH) and temperature (Zobrist et

48   al., 2008; Mikhailov et al., 2009). Ambient and laboratory-generated SOA particles have been

49   observed to bounce off the smooth hard surface of an inertial impactor at low RH, implying a

50   non-liquid state (Virtanen et al., 2010; Saukko et al., 2012; Bateman et al., 2015; Jain and

51   Petrucci, 2015), whereas predominantly biogenic SOA particles in the Amazon basin did not

52   bounce off the impactor surface at high RH, implying they are primarily liquid (Bateman et al.,

53   2016). Upon dilution or heating, SOA particles were observed to evaporate unexpectedly slowly,

54   consistent with their (semi-)solid phases (Cappa and Wilson, 2011; Vaden et al., 2011; Yli-Juuti

55   et al., 2017). Direct measurements of viscosity of SOA bulk material derived from oxidation of

56   α-pinene (Renbaum-Wolff et al., 2013; Zhang et al., 2015; Hosny et al., 2016), limonene (Hinks

57   et al., 2016), isoprene (Song et al., 2015), and toluene (Song et al., 2016a) have confirmed that

58   SOA particles adopt a wide range of viscosities.

59   The particle phase state has been shown to affect gas uptake and chemical transformation of

60   organic compounds due to kinetic limitations of bulk diffusion (Shiraiwa et al., 2011; Abbatt et

Atmospheric
Chemistry
and Physics
Discussions

Open Access

EGU

61   al., 2012; Kuwata and Martin, 2012; Zhou et al., 2013; Slade and Knopf, 2014; Arangio et al.,

62   2015; Davies and Wilson, 2015; Wang et al., 2015; Berkemeier et al., 2016; Marshall et al.,

63   2016). Molecular motion can be hindered in a highly viscous matrix, slowing down

64   photochemical reactions in particles (Lignell et al., 2014; Hinks et al., 2016). Partitioning of

65   semi-volatile compounds into viscous particles may result in kinetically-limited growth in

66   contrast to quasi-equilibrium growth (Perraud et al., 2012; Shiraiwa and Seinfeld, 2012; Shiraiwa

67   et al., 2013; Booth et al., 2014; Zaveri et al., 2014; Liu et al., 2016). Water diffusion can be still

68   fast even in an amorphous solid matrix under room temperature, but it can be hindered

69   significantly under low temperatures (Mikhailov et al., 2009; Zobrist et al., 2011; Bones et al.,

70   2012; Berkemeier et al., 2014; Price et al., 2014), affecting homogeneous vs. heterogeneous ice

71   nucleation pathways (Murray et al., 2010; Wang et al., 2012; Baustian et al., 2013; Schill and

72   Tolbert, 2013; Berkemeier et al., 2014; Schill et al., 2014; Lienhard et al., 2015; Ignatius et al.,

73   2016). Despite the substantial implications of the SOA particle phase state, its effects on gas-

74   particle interactions have not yet been considered explicitly in current climate and air quality

75   models (Shrivastava et al., 2017).

76   Group contribution methods have been used to predict the viscosities of pure compounds.

77   Song et al. (2016) showed that estimations from group contribution approaches combined with

78   either nonideal or ideal mixing reproduced the RH-dependent trends particularly well for the

79   alcohol, di-, and tricarboxylic acid systems with viscosity of up to 10^4 Pa s. By contrast, model

80   calculations overestimated the viscosity of more viscous compounds including mono-, di-, and

81   trisaccharides by many orders of magnitude (Song et al., 2016b). A recent study compiled

82   viscosity of organic compounds with atmospherically relevant functional groups, investigating

83   the influence of the number and location of functional groups on viscosity (Rothfuss and Petters,

Atmospheric
Chemistry
and Physics
Discussions

Open Access

EGU

84   2017). Information on molecular structures, however, is often difficult to obtain in laboratory or

85   field measurements on atmospheric aerosols.

86   Particle phase state can be characterized by a glass transition temperature (T_g), which is a

87   characteristic temperature representing a non-equilibrium phase transition from a glassy solid

88   state to a semi-solid state as the temperature increases (Koop et al., 2011). Recently, we have

89   developed a method to estimate T_g of pure organic compounds comprised of carbon, hydrogen,

90   and oxygen (CHO compounds) with molar mass less than 450 g mol^{-1} based on their molar mass

91   and atomic O:C ratio (Shiraiwa et al., 2017). It has been applied successfully in a global

92   chemistry climate model to predict T_g and the phase state of atmospheric SOA. Global

93   simulations indicate that SOA particles are mostly liquid or semi-solid in the planetary boundary

94   layer, while they should be glassy in the middle and upper troposphere (Shiraiwa et al., 2017). A

95   very recent study provided a consistent result, suggesting that mixing timescales of organic

96   molecules within SOA are often < 1 h in a global planetary boundary layer (Maclean et al.,

97   2017).

98   It has been shown that SOA particles contain oligomeric compounds with molar masses

99   higher than 450 g mol^{-1} (Gao et al., 2004; Tolocka et al., 2004; Nizkorodov et al., 2011; Nozière

100   et al., 2015), which makes the previously developed parameterization incomplete. In this study,

101   we extend the parameterization of T_g to higher molar mass compounds, and apply it to high-

102   resolution mass spectrometry data for toluene SOA and biomass burning particles. The

103   Arrhenius approach and the Gordon-Taylor mixing rules were applied to estimate viscosity of

104   SOA bulk materials to compare with the literature reported viscosity measurements. This method

105   will be useful for estimations of viscosity of organic particles, for which high-resolution mass

106   spectra are available. It can also be applied in global or regional models to evaluate impacts of

107   the particle phase state on the role of SOA in climate and air quality.

108

109   **2. Parameterization development**

110   **2.1 Glass transition temperature**

111   Figure 1a shows the dependence of T_g on the molar mass (M) of organic compounds. Solid

112   markers represent measured T_g of 258 CHO compounds (Koop et al., 2011; Dette et al., 2014;

113   Rothfuss and Petters, 2017), while open markers represent 654 CHO compounds in SOA

114   (Shiraiwa et al., 2014). Markers are color-coded by atomic O:C ratio. Their melting points (T_m)

115   were estimated by the Estimation Programs Interface (EPI) Suite software version 4.1 (US-EPA,

116   2012) and their T_g were estimated using the Boyer-Kauzmann rule: $T_g = g \cdot T_m$ with $g = 0.7$ (Koop

117   et al., 2011; Shiraiwa et al., 2017). A subset of data shown in Figure 1 was originally published

118   in Shiraiwa et al. (2017) for compounds with $M < 450$ g mol^{-1}. This version of the figure has

119   been updated to include a number of experimentally measured T_g values of larger compounds

120   with M up to 1153 g mol^{-1}, including aliphatic compounds containing OH and/or COOH groups.

121   Specifically, data for 76 aliphatic alcohols, 39 carbohydrates and their derivatives, 4 carboxylic

122   acids, and 4 hydroxy acids, as compiled by Rothfuss and Petters (2017), have been added to

123   Figure 1. These updates are critical for reliable parametrization of T_g based on M. When M

124   increases above ~500 g mol^{-1}, the slope of T_g decreases, making it challenging to extrapolate the

125   low-M data from the original Shiraiwa et al. (2017) study to higher M values. When M increases

126   to ~1000 g mol^{-1}, the corresponding T_g appears to level at around 420 K.

127   Such dependence on M has been described for polymers with the Fox-Flory equation:

128    $T_g(M) = T_{g,\infty} - \frac{K_m}{M}$ (Fox Jr and Flory, 1950), where K_m is a constant and $T_{g,\infty}$ is the asymptotic

Atmospheric
Chemistry
and Physics
Discussions

Open Access

129   value of T_g specific to the polymer. We conducted a literature search and found that most of the

130   reported $T_{g,\infty}$ values fell below ~500 K (Fox Jr and Flory, 1950; Onder et al., 1972; Montserrat

131   and Colomer, 1984; Polymer handbook, 1999; Papadopoulos et al., 2004; Matsushima et al.,

132   2017). The Fox-Flory equation works very well for high molar mass compounds and is also

133   generally applicable to smaller compounds (Koop et al., 2011), as supported by an approximately

134   linear dependence of T_g on the inverse molar mass in Fig. A1. Figure 1b plots the values of T_g as

135   a function of the atomic O:C ratio of organic molecules. Figures 1a and 1b clearly demonstrate

136   that T_g depends primarily on the molar mass with a weak dependence on the atomic O:C ratio.

137   A parameterization for T_g calculation based on the molar mass and atomic O:C ratio was

138   developed in our recent work, which is applicable to CH and CHO compounds with $M < 450$ g

139   mol^{-1} (Shiraiwa et al., 2017):

140            $$T_g = A + BM + C^2M^2 + D\,(O:C) + E\,M\,(O:C) \tag{1}$$

141   where A = –21.57 (±13.47) [K], B = 1.51 (±0.14) [K mol g^{-1}], C = -1.7×10^{-3} (±3.0×10^{-4}) [K

142   mol^2 g^{-2}], D = 131.4 (±16.01) [K] and E = –0.25 (±0.085) [K mol g^{-1}], respectively. These values

143   were obtained by fitting the measured T_g of 179 CH and CHO compounds with $M < 450$ g mol^{-1}

144   with multi-linear least squares analysis. Note that application of Eq. (1) may provide

145   unreasonable T_g values for compounds with $M > 500$ g mol^{-1} because it does not account for the

146   strong curvature in the T_g vs. M dependence shown in Figure 1a.

147   In this study we have developed an improved parameterization to predict T_g of CH and

148   CHO compounds using the number of carbon (n_C), hydrogen (n_H), and oxygen (n_O) that can also

149   be applied to higher molar mass compounds. Motivated by a good correlation between T_g and

150   volatility (Fig. 1a in Shiraiwa et al., (2017)), we use an equation with a similar formulation to the

Atmospheric
Chemistry
and Physics
Discussions

151   equation used to predict the saturation mass concentration or volatility (Donahue et al., 2011; Li

152   et al., 2016):

153    $T_g = (n_C^0 + ln(n_C))\, b_C + ln(n_H)\, b_H + ln(n_C)\, ln(n_H)\, b_{CH} + ln(n_O)\, b_O + ln(n_C)\, ln(n_O)\, b_{CO}$ (2)

154   where n_C^0 is the reference carbon number, b_C, b_H and b_O denote the contribution of each atom to

155   T_g, and b_{CH} and b_{CO} are coefficients that reflect contributions from carbon-hydrogen and carbon-

156   oxygen bonds, respectively. These values were obtained by fitting the measured T_g of 42 CH

157   compounds and 258 CHO compounds with multi-linear least squares analysis with 68%

158   prediction and confidence intervals. The best-fit parameters are summarized in Table 1.

159   Note that the evaluation dataset used to derive Eq. (2) contains CH compounds with $M <$

160   260 g mol^{-1} (see Fig. A2a for comparison of measured and predicted T_g). Thus, the application of

161   Eq. (2) to higher molar mass CH compounds may require further investigations when measured

162   T_g for higher molar mass CH compounds becomes available. Figure 1c shows that the T_g values

163   predicted using Eq. (2) are in good agreement with the T_g values measured in experiments (see

164   also Fig. A2b) or estimated by the Boyer-Kauzmann rule as indicated by the high correlation

165   coefficient of 0.95. T_g of individual compounds can be predicted within ±21 K as indicated by

166   the prediction band (dotted lines in Fig. 1c); however, this uncertainty may be much smaller for

167   multicomponent SOA mixtures under ideal mixing conditions as indicated in the confidence

168   band (dashed lines, almost overlapping with the 1:1 line).

169   These results are noteworthy given that the parameterization (Eq. 2) does not consider

170   either explicit molecular structures or functional groups. Previous studies have shown that T_g can

171   be especially sensitive to the number of OH groups, which interact strongly through hydrogen

172   bonding. For example, Nakanishi et al., (2011) found a direct relationship between T_g and the

173   number of hydroxyl groups in a molecule for sugar alcohols; T_g increases as the number of OH

Atmospheric
Chemistry
and Physics
Discussions

174   groups increases. They reported that the correlation between T_g and the number of OH groups

175   was much stronger than the correlation between T_g and the number of carbons in a molecule.

176   Such a trend is implicitly included in Eq. (1) and (2), which contain the O:C ratio and number of

177   oxygen atoms as parameters, respectively. Recently, Rothfuss and Petters (2017) showed an

178   approximately linear relationship between the number of OH groups and T_g for compounds with

179   up to eight OH groups. Grayson et al. (2017) showed that addition of hydroxyl functional groups

180   increases viscosity, a conclusion supported by both the experimental data and quantitative

181   structure-property relationship model. The correlation between T_g and the number of carbon

182   atoms is consistent with the free volume theory, while the correlation with the number of OH

183   groups is more consistent with the topological constraint theory (Nakanishi and Nozaki, 2011;

184   van der Sman, 2013). Future experiments targeting more comprehensive T_g data, especially for

185   higher molar mass compounds, would lead to further refinements of our T_g parameterizations.

186   Comparing Eq. (1) and (2), the two parameterizations give similar performance for

187   compounds with $M < 450$ g mol^{-1} as shown in Fig. A2c. The statistical measures of correlation

188   coefficient (R), mean bias (MB), and root mean square error (RMSE) are 0.93, –6.45 K, and

189   25.64 K, respectively, for the performance of Eq. (1), while for Eq. (2), they are 0.95, 3.15 K,

190   and 21.11 K, respectively. It should be noted again that Eq. (1) cannot be used to predict T_g for

191   compounds with $M > 450$ g mol^{-1}. For example, T_g of stachyose ($M = 667$ g mol^{-1}) predicted by

192   Eq. (1) is 198 K, while that by Eq. (2) is 394 K, which agrees much better with the measured

193   mean T_g of 396 K (Rothfuss and Petters, 2017). Eq. (2) is more flexible than Eq. (1) and can be

194   potentially expanded to include compounds containing hetero-atoms (e.g., nitrogen or sulfur),

195   once substantial sets of experimental values of T_g for such compounds become available.

196   Regarding the application in air quality and climate models, Eq. (1) can be applied in the

Atmospheric
Chemistry
and Physics
Discussions

197   volatility basis set (VBS) (Donahue et al., 2006; Donahue et al., 2011) and the molecular

198   corridor approach (Shiraiwa et al., 2014; Li et al., 2016) to predict the T_g of SOA particles

199   (Shiraiwa et al., 2017), while the new parameterization may be suitable for coupling with the

200   statistical oxidation model which characterizes the SOA evolution as a function of n_C and n_O

201   (Cappa and Wilson, 2012; Jathar et al., 2015).

202   These parameterizations (Eqs. 1, 2) calculate T_g based on the elemental composition of

203   organic compounds. SOA particles contain a number of organic compounds as well as a variable

204   amount of liquid water. Estimations of T_g for SOA-water mixtures were discussed by Shiraiwa et

205   al. (2017), who applied the Gordon-Taylor equation validated for a wide range of mixtures of

206   organics, polymer, and water (Roos, 1993; Hancock and Zografi, 1994; Zobrist et al., 2008;

207   Dette et al., 2014; Dette and Koop, 2015). Briefly, T_g of mixtures of SOA compounds under dry

208   conditions ($T_{g,org}$) were calculated assuming the Gordon-Taylor constant (k_{GT}) of 1 (Dette et al.,

209   2014): $T_{g,org} = \sum_i w_i T_{g,i}$, where w_i is the mass fraction of organic compound i, which can be

210   derived using mass concentrations of SOA products. Under humid conditions, SOA particles

211   take up water by hygroscopic growth in response to RH. The Gordon-Taylor equation can also

212   be applied to calculate T_g of organic-water mixtures considering the mass fraction of organics

213   (w_{org}) in SOA particles (Koop et al., 2011):

214    $$T_g(w_{org}) = \frac{(1-w_{org})T_{g,w} + \frac{1}{k_{GT}}w_{org}T_{g,org}}{(1-w_{org}) + \frac{1}{k_{GT}}w_{org}}$$ (3)

215   w_{org} can be calculated using the mass concentrations of water (m_{H_2O}) and SOA (m_{SOA}) as $w_{org} =$

216    $m_{SOA} / (m_{SOA} + m_{H_2O})$. m_{H_2O} can be estimated using the effective hygroscopicity parameter (κ)

217   (Petters and Kreidenweis, 2007):

218    $$m_{H2O} = \frac{\kappa \rho_w m_{SOA}}{\rho_{SOA}\left(\frac{1}{a_w}-1\right)}$$ (4)

Atmospheric
Chemistry
and Physics
Discussions

219   The density of water (ρ_w) is 1 g cm^{-3}, the density of SOA particles (ρ_{SOA}) is assumed to be 1.2 g

220   cm^{-3} (Kuwata et al., 2012), m_{SOA} is the total mass concentrations of SOA, and a_w is the water

221   activity calculated as a_w = RH/100.

222

223   **2.2 Viscosity**

224   Temperature dependence of viscosity (η) was predicted using the modified Vogel-

225   Tammann-Fulcher (VTF) equation (Angell, 1991):

226
$$\eta = \eta_\infty e^{\frac{T_0 D}{T-T_0}}$$
(3)

227   where η_∞ is viscosity at infinite temperature; T_0 is the Vogel temperature; T is the ambient

228   temperature. The fragility parameter, D, characterizes how rapidly the dynamics of a material

229   slow down as T approaches T_g, reflecting to what degree the temperature dependence of the

230   viscosity deviates from Arrhenius behavior. When T is close to T_g ($T_g/T \approx 1$), smaller D values

231   indicate that viscosity is sensitive to temperature change (fragile behavior); while larger D values

232   indicate that viscosity is less sensitive to temperature change (strong or Arrhenius behavior).

233   Assuming $\eta_\infty = 10^{-5}$ Pa s (Angell, 1991):

234
$$\log \eta = -5 + 0.434 \frac{T_0 D}{T-T_0}$$
(4)

235   When $T = T_g$, $\eta = 10^{12}$ Pa s, which leads to (Angell, 1991; Angell, 2002):

236
$$T_0 = \frac{39.17\, T_g}{D+39.17}$$
(5)

237   As can be seen in Eq. (5), both T_g and D are required to calculate η from Eq. (4) at a given

238   temperature.

239   Figure 2 shows the T_g-scaled Arrhenius plot of fragility (viscosity versus T_g/T) referred to

240   as an Angell plot (Angell, 1995). D values of organic compounds are typically in the range of

241   ~5–30 (Angell, 1997). To estimate D values that could be applied to SOA compounds, we

242   compiled measured fragility values. Fragility was often measured in the form of the fragility

243   steepness index (m), which represents the slope of the Arrhenius plot at the point where $T = T_g$

244   (Boehmer et al., 1993). Compounds with lower m exhibit higher D values, indicating stronger

245   glass formers. The measured m of 95 organic compounds are included in the Supplement. m can

246   be converted to D using the following equation (see the full derivation of this equation in

247   Appendix A):

248
$$D = \frac{665.89}{m - 17} \qquad (6)$$

249   Figure 3 shows the measured D as a function of (a) molar mass and (b) atomic O:C ratio

250   of organic molecules. The molar mass exerts a stronger effect on fragility, while there is little

251   dependence of D on the O:C ratio. As molar mass increases, D approaches a lower limit of 10.3

252   ($\pm$ 1.7), consistent with the value of 10 used in our recent study (Shiraiwa et al., 2017). To

253   evaluate the impact of the variations of D on viscosity prediction, sensitivity calculations were

254   conducted as described in Sect. 3.

255   Besides the VTF equation, another commonly used equation for describing the

256   temperature dependence of viscosity is the Williams-Landel-Ferry (WLF) equation: $\log \frac{\eta(T)}{\eta(T_g)} =$

257    $\frac{-C_1(T - T_g)}{C_2 + (T - T_g)}$, where empirical parameters C_1 and C_2 are adopted as 17.44 and 51.6 K, respectively

258   (Williams et al., 1955; Schill and Tolbert, 2013; Wang et al., 2015). The two equations are

259   mathematically equivalent and the WLF and VTF parameters are related through $C_1 =$

260    $\frac{DT_0}{2.303(T_g - T_0)}$ and $C_2 = T_g - T_0$. It is shown that, compared to the WLF equation, the VTF

261   parameterization does not rely heavily on the free volume assumption and the Vogel temperature

262   T_0 has a more profound physical meaning that relates both thermodynamic and kinetic concepts

263   (O'Connell and McKenna, 1999; Huang and McKenna, 2001). The calculations of viscosity in

Atmospheric
Chemistry
and Physics
Discussions

264   this study are based mainly on the VTF equation and the difference between calculated results

265   from the two equations will be briefly discussed in the following section.

266

267   **3. Comparison of predicted viscosity with measurements**

268   **3.1. SOA formed from α–pinene and isoprene**

269   The purpose of this section is to demonstrate that viscosity of SOA material can be

270   predicted over a broad range of RH values from four parameters: T_g of dry SOA ($T_{g,org}$), fragility

271   (D), hygroscopicity (κ), and the Gordon-Taylor constant for mixing SOA and water (k_{GT}).

272   Viscosity of α-pinene SOA has been measured as a function of RH by several groups using

273   multiple experimental techniques as shown in Fig. 4(a) (Abramson et al., 2013; Renbaum-Wolff

274   et al., 2013; Kidd et al., 2014; Pajunoja et al., 2014; Bateman et al., 2015; Zhang et al., 2015;

275   Grayson et al., 2016). These datasets suggest that viscosity of α-pinene SOA is very high ($\sim > 10^8$

276   Pa s) at low RH and decreases with an increase in RH reaching a value of ~10 Pa s at 80% RH.

277   As can be seen in Fig. 4(b), isoprene SOA is less viscous with $\eta < 10^6$ Pa s even under dry

278   conditions, undergoing a phase transition from a semi-solid phase to a liquid phase at ~55% RH

279   (Bateman et al., 2015; Song et al., 2015).

280   The solid lines with the shaded areas in Figure 4 are viscosity values predicted using

281    $T_{g,org}$, D, κ, k_{GT}. $T_{g,org}$ values were adopted by Berkemeier et al. (2014) who estimated $T_{g,org}$ with

282   the Boyer-Kauzmann rule using the melting point of representative SOA oxidation products.

283   Note that Eq. (1) or (2) were not used to estimate $T_{g,org}$, which should be done in future studies

284   by obtaining their elemental composition using high resolution mass spectrometry. For α-pinene,

285    $T_{g,org}$ was assumed to be 278 K corresponding to an O:C ratio of 0.5 (Berkemeier et al., 2014),

286   which is a typical O:C ratio of α-pinene SOA (Aiken et al., 2008; Chen et al., 2011; Putman et

Atmospheric
Chemistry
and Physics
Discussions

287   al., 2012). The wide range of viscosities reported for α-pinene SOA may indicate that the O:C

288   values may be different in different experiments. $T_{\text{g,org}}$ selected for isoprene SOA was 255 K,

289   corresponding to the O:C ratio of 0.6. Although no measurements of the O:C ratio for the

290   experimental isoprene SOA data were reported, Song et al. (2015) estimated O:C of 0.64-1.1

291   based on literature values. As O:C ratios are useful in estimating $T_{\text{g,org}}$, we encourage the

292   measurement of the O:C ratio of SOA when conducting viscosity measurements.

293   For both α-pinene and isoprene SOA, D was set to 10 based on the analysis presented in

294   Fig. 3(a). κ was set to 0.1 based on field and laboratory measurements (Gunthe et al., 2009;

295   Lambe et al., 2011b; Pajunoja et al., 2014; Petters et al., 2017) and k_{GT} was assumed to be 2.5

296   (Zobrist et al., 2008; Koop et al., 2011). Using these parameters, the predicted viscosities match

297   well the magnitude and the RH-dependence of the measured viscosity of α-pinene and isoprene

298   SOA. Figure 4 also shows predicted viscosities (dotted lines) using the WLF equation, which

299   shows similar values as the VTF equation, but slightly underestimates the viscosity of α-pinene

300   SOA at low RH and overestimates the viscosity of isoprene SOA at high RH.

301   Sensitivity studies were conducted to examine the effects of $T_{\text{g,org}}$, D, κ and k_{GT}, on the

302   calculated viscosity. In these studies, $T_{\text{g,org}}$ of α-pinene and isoprene SOA were varied within 229

303   - 328 K and 255 - 316 K, respectively, representing $T_{\text{g,org}}$ of different oxidation states

304   (Berkemeier et al., 2014). D was varied between 5 and 30, which is the range characteristic for

305   organic compounds (see Fig. 3a). κ of 0.05 - 0.15 were used for α-pinene and isoprene SOA

306   (Lambe et al., 2011b; Pajunoja et al., 2015). For the Gordon-Taylor constant, values of 2.5±1.5

307   were considered (Zobrist et al., 2008; Koop et al., 2011; Dette et al., 2014; Dette and Koop,

308   2015).

Atmospheric
Chemistry
and Physics
Discussions

309   The effect of varying each parameter on the calculated viscosity of α-pinene SOA is

310   illustrated in Fig. 5. Variations of ±50 K in $T_{g,org}$ result in 3-6 orders of magnitude difference in

311   calculated values at dry conditions, indicating that $T_{g,org}$ is a critical parameter for viscosity

312   estimations. Decreasing D from 10 to 5 led to a decrease of calculated values by more than one

313   order of magnitude. The calculated results were within the upper limit of measurements when

314   increasing D from 10 to 20, and the predicted values were only slightly enhanced when further

315   increasing D from 20 to 30. Calculated values with variations in κ from 0.05 to 0.15 and k_{GT}

316   from 1.0 to 4.0 were all within the measured ranges.

317   For isoprene SOA, an increase of $T_{g,org}$ to 287 K, which represents a higher oxidation

318   state (Berkemeier et al., 2014), led to calculated values to be several orders of magnitude higher

319   than the upper limit of measurements (Fig. 6a). When $T_{g,org}$ reaches 316 K, isoprene SOA can

320   occur as a solid for RH lower than ~40%. Compared to α-pinene SOA, a variation in D has a

321   larger effect on the calculated viscosity (Fig. 6b). For a range of 5 - 30 for D, calculations with

322   the D value of 10 agreed well with the measurements, while other D values resulted in calculated

323   viscosity outside of the measured ranges. Figures 6c and 6d show that decreasing κ and k_{GT}

324   below the reference values, the predictions overestimate the measured η by one or two orders of

325   magnitude. The latter is most evident at RH > 60%, where the calculated values were higher than

326   the upper limit of measurements. Modeling results with κ and k_{GT} increasing to 0.15 and 4.0,

327   respectively, were within the lower limit of measurements.

328   The above comparison between the measured and predicted viscosity demonstrates that

329   the method described in this study can reproduce reasonably well the measured RH-dependent

330   viscosity of SOA formed from α-pinene and isoprene. The sensitivity calculations showed that

331       $T_{g,org}$ contributed the most to the uncertainty in the viscosity estimates. Previous studies have

Atmospheric
Chemistry
and Physics
Discussions

332   shown that the experimental conditions such as particle mass concentrations (Grayson et al.,

333   2016) and RH upon SOA formation (Kidd et al., 2014) can impact chemical composition of SOA

334   and hence the viscosity. Further efforts to constrain the uncertainties are needed both in

335   experiments and parameterizations.

336

337   **3.2. SOA formed from toluene**

338   In this and the following sections, we examine the feasibility of calculating the value of

339    $T_{g,org}$ from mass spectrometry data on SOA. Hinks et al. (2017) measured the elemental

340   composition of toluene SOA using nanospray desorption electrospray ionization high-resolution

341   mass spectrometry (nano-DESI-HRMS) (Roach et al., 2010a, b). Toluene SOA were formed by

342   OH photooxidation in an aerosol smog chamber at <2% RH (mass loading = 23 μg m^{-3}) and 75%

343   RH (mass loading = 8 μg m^{-3}) to investigate the effect of RH on the chemical composition of

344   toluene SOA formed under low-NO$_x$ conditions. Measurements revealed a significant reduction

345   in the fraction of oligomers present in toluene SOA generated under high RH conditions

346   compared to SOA generated under low RH conditions (Hinks et al., 2017). The detected molar

347   mass of individual oxidation products spanned a range of 102 - 570 g mol^{-1} at high RH, which

348   increased up to 726 g mol^{-1} at low RH.

349   Figure 7(a) shows the interdependence of glass transition temperature, volatility, and

350   molar mass. Glass transition temperatures of detected compounds were calculated using Eq. (2).

351   Saturation mass concentrations or volatilities of detected compounds were estimated from the

352   elemental composition by using the parameterization of Li et al. (2016). The analysis is based on

353   the molecular corridor approach—a two-dimensional framework of volatility and molar mass of

354   SOA components constrained by boundary lines of low and high atomic O:C ratio,

Atmospheric
Chemistry
and Physics
Discussions

355   corresponding to n-alkanes (C_nH_{2n+2}, O:C = 0) and sugar alcohols ($C_nH_{2n+2}O_n$, O:C = 1),

356   respectively (Shiraiwa et al., 2014; Li et al., 2016). The toluene SOA constituents are well

357   constrained by the molecular corridor and T_g are higher for compounds with higher molar mass

358   and lower volatility.

359   Eq. (1) was used to calculate T_g for individual compounds with $M < 450$ g mol^{-1}, while

360   excluding compounds with molar mass higher than 450 g mol^{-1}. This approach was deemed

361   reasonable as such high molar mass compounds account for < 10% of all toluene SOA products

362   formed at low RH, and for < 2% formed at high RH. Eq. (2) was used to calculate T_g for all the

363   detected compounds. T_g of dry toluene SOA ($T_{g,org}$) was then computed using the Gordon-Taylor

364   approach with $k_{GT} = 1$ (Sect. 2.1). The relative mass concentrations of individual components

365   were assumed to be proportional to their relative abundance in the nano-DESI-HRMS spectrum.

366   This assumption has a number of caveats (Bateman et al., 2012; Nguyen et al., 2013), and as we

367   will see below, it results in deviations between the predicted and measured viscosity. Table 2

368   summarizes the results of such calculations, showing that the $T_{g,org}$ by Eq. (1) – excluding high

369   molar mass compounds – is about 10 K lower as compared to $T_{g,org}$ by Eq. (2). $T_{g,org}$ at low RH is

370   predicted to be higher than $T_{g,org}$ at high RH, which results from a lower abundance of high molar

371   mass compounds observed at high RH. This trend is consistent with Kidd et al. (2014), who

372   showed that SOA material formed under dry conditions is more viscous than that formed under

373   wet conditions.

374   Figure 7(b) shows the predicted viscosity of toluene SOA as a function of RH, as

375   compared to the measured viscosity of toluene SOA formed in an oxidation flow reactor at 13%

376   RH and two mass loading ranges (60 - 100 μg m^{-3} and 600 - 1000 μg m^{-3}) (Song et al., 2016a).

377   Indirect viscosity measurements are also included in shaded boxes (Bateman et al., 2015; Li et

378   al., 2015). Lines with shaded areas are calculated viscosities using $T_{g,org}$ as described above. κ

379   was assumed to be 0.25 based on laboratory measurements (Lambe et al., 2011a; Hildebrandt

380   Ruiz et al., 2015). For achieving good fit, D was set to 13 and k_{GT} was assumed to be 3.0 (Dette

381   et al., 2014). Estimations with Eq. (1) match the measured viscosity values very well over the

382   entire RH range. Predictions with Eq. (2) overestimated the measurements by one or two orders

383   of magnitude at moderate RH between 30% and 50%, while they agreed with the measurements

384   derived at RH ≥ 60% and at the dry conditions.

385   There are several possible reasons for the difference between the measurements and

386   predictions. First, the relative abundance of high molar mass compounds observed in HRMS

387   measurements may be overestimated, as high molar mass compounds tend to have higher (yet

388   generally unknown) ionization efficiencies compared to lower molar mass compounds. Second,

389   the nano-DESI-HRMS analysis of toluene SOA was limited to m/z range of 100 -1000 (Hinks et

390   al., 2017). It is possible that some SOA products with lower molar mass were present in particles

391   but not detected, which would lead to an overestimation of T_g. Third, the chemical composition

392   of toluene SOA are likely different between Hinks et al. (2017) and Song et al. (2016) because of

393   the differences in the experimental conditions. Specifically, toluene SOA was formed in a Teflon

394   chamber in Hinks et al., while Song et al. used an oxidation flow reactor to generate toluene

395   SOA. The O:C ratios are 0.71 at low RH and 0.63 at high RH based on nano-DESI-HRMS

396   measurements in Hinks et al. (2017), while it was 1.06 based on the aerosol mass spectrometry

397   (AMS) measurements in Song et al. (2016). Simultaneous measurements of viscosity and

398   chemical composition should be performed in future studies.

399

400   **3.3 Biomass Burning Particles**

Atmospheric
Chemistry
and Physics
Discussions

401   To further explore the applicability of our viscosity prediction method using elemental

402   composition as measured by HRMS, we performed similar calculations for biomass burning

403   organic particles emitted from test facility burns of subalpine fir and lodgepole pine trees,

404   conducted as a part of the FIREX 2016 campaign (Selimovic et al., 2017). These samples were

405   analyzed by HRMS using two different ionization sources: electrospray ionization (ESI) and

406   atmospheric pressure photoionization (APPI). Mass spectra shown in Fig. 8(a) and (b) indicate

407   that a substantial number of compounds were detected by both methods (109 and 170

408   compounds for subalpine fur and lodgepole pine, respectively). However, pronounced

409   differences are also observed between the ESI and APPI spectra both in terms of the identity and

410   signal intensities of the detected compounds.

411   Glass transition temperatures for the assigned CH and CHO compounds were computed

412   using Eq. (2). Nitrogen and sulfur containing compounds (CHON and CHOS) are not yet

413   covered by Eq. (2) and were therefore excluded from the analysis. The exclusion is justified

414   because in the selected samples, CHON and CHOS compounds comprised less than 10% of the

415   detected ion intensity and <15% of the assigned compounds. T_g of organic mixtures ($T_{g,org}$) were

416   then calculated using the Gordon-Taylor approach with $k_{GT} = 1$, assuming that the relative

417   concentration of each compound is proportional to its MS signal intensity. The calculated $T_{g,org}$

418   values for the mixtures are specified in the legend of Figure 9. For both types of mixtures, the

419   calculated $T_{g,org}$ for the APPI MS data is lower than the value calculated based on the ESI MS

420   data with a difference of 32 K for subalpine fir and 11 K for the lodgepole pine. Figure 9 shows

421   the predicted viscosity as a function of RH, assuming $D = 10$, $\kappa = 0.10$ and $k_{GT} = 2.5$ The

422   difference in $T_{g,org}$ derived from ESI and APPI results in a variation of predicted viscosity at low

423   RH by up to five and two orders of magnitude for subalpine fir and lodgepole pine, respectively.

Atmospheric
Chemistry
and Physics
Discussions

Open Access

424   The difference in the calculated $T_{g,org}$ values is attributed to the chemical profile of the

425   species detected using different ionization techniques as shown in mass spectra in Fig. 8(a) and

426   (b). Van Krevelen diagrams in Fig. 8(c) and (d) illustrate these compositional differences

427   between chemical species detected by ESI and APPI. ESI is more efficient at detection of polar

428   compounds (Kiontke et al., 2016), which typically have higher O:C ratios and therefore would

429   result in higher predicted values of viscosity (Koop et al., 2011; Saukko et al., 2012). APPI

430   enables the detection of nonpolar compounds with lower O:C ratios, in particular polycyclic

431   aromatic hydrocarbons (PAHs), that have low ionization efficiencies when analyzed by ESI MS

432   (Raffaelli and Saba, 2003; Itoh et al., 2006). Due to the complementary nature of these ionization

433   methods, it is most likely that the actual glass transition temperature and viscosity of each type of

434   SOA are somewhere in between the values inferred from ESI and APPI data sets: ESI MS may

435   be viewed as providing the upper limit of viscosity, while APPI MS gives the lower limit. Our

436   results indicate that the use of complementary ionization techniques may help evaluate the

437   associated uncertainty for the prediction of viscosity values based on the elemental composition

438   as measured by HRMS.

439

440   **4 Conclusion**

441   We have developed a parameterization for calculation of the glass transition temperature

442   of individual SOA compounds with molar mass up to ~1100 g mol^{-1} using the number of carbon,

443   oxygen, and hydrogen atoms. Viscosity of SOA was estimated using the T_g-scaled Arrhenius plot

444   of viscosity versus T_g/T and the Gordon-Taylor approach to account for mixtures of SOA and

445   water. The fragility parameter D was compiled for organic compounds and we found that D

446   approaches a lower limit of ~10 (+/- 1.7) as the molar mass increases. The resulting viscosity

Atmospheric
Chemistry
and Physics
Discussions

447   estimations agree well with measured viscosity of α-pinene and isoprene SOA, validating our

448   method. Using HRMS data, glass transition temperatures of individual components and viscosity

449   of toluene SOA were predicted, also resulting in a good agreement with measurements.

450   However, we note that the predicted viscosities were slightly higher than the measured values

451   suggesting that additional considerations may need to be taken into account. For example, the

452   ionization efficiency of both low and high molar mass compounds may have a pronounced effect

453   on the relative abundance of different classes of compounds in HRMS data. The viscosity

454   prediction method was also applied to biomass burning particles, whose elemental composition

455   was measured using HRMS with two different ionization techniques. Substantial differences in

456   viscosity estimations were obtained using ESI and APPI mass spectra.

457   Figure 10 summarizes the predicted range of viscosity of α-pinene SOA, isoprene SOA,

458   toluene SOA, and biomass burning particles. Isoprene SOA has lower viscosity, reflecting lower

459   glass transition temperature due to relatively low molar mass of isoprene oxidation products. α-

460   pinene and toluene SOA have much higher viscosity with a different shape of the RH

461   dependence due to differences in glass transition temperatures and hygroscopicity. Biomass

462   burning particles have moderate viscosity between the two extreme cases. Currently, both

463   predictions and measurements are subject to large uncertainties and variations. Complementary

464   measurements of viscosity and chemical composition employing different ionization techniques

465   are desired to further constrain RH-dependent viscosity in future studies. Current T_g

466   parameterizations do not consider functionality or molecular structure explicitly and further

467   measurements of T_g and viscosity of SOA would allow us to refine the method presented in this

468   study. Nevertheless, current results offer a promising starting point and such simple

469   parameterizations are practical for predicting viscosity of particles as measured by HRMS. The

470   developed viscosity prediction method should also be useful in recent efforts of simulating the

471   distribution of SOA phase state and related properties in regional or global air quality models

472   (e.g., Maclean et al., 2017; Shiraiwa et al., 2017).

473

474   **Appendix A: Conversion of fragility steepness index (*m*) to fragility (*D*)**

475   Fragility steepness index (*m*) is defined as:

476    $$m = \lim_{T \to Tg} \frac{d \, log\eta}{d(T_g/T)} \tag{A1}$$

477   Combining Eq. (A1) with Eq. (4) gives:

478    $$m = \lim_{T \to Tg} \frac{d}{d(T_g/T)} \left(-5 + 0.434 \frac{T_0 D}{T - T_0} \right) \tag{A2}$$

479   Considering that $\eta = 10^{12}$ Pa s at $T = T_g$ (Angell, 1991), and by defining $\Delta x = 1 - T_g/T$, and a

480   combination with Eq. (5) leads to:

$$m = \lim_{\Delta x \to 0} \frac{1}{\Delta x} \left(12 - \left(-5 + 0.434 \frac{\frac{39.17 \, T_g}{D + 39.17} D}{\frac{T_g}{1 - \Delta x} - \frac{39.17 \, T_g}{D + 39.17}} \right) \right)$$

$$= \lim_{\Delta x \to 0} \frac{1}{\Delta x} \left(17 - 0.434 \frac{39.17 T_g D(1 - \Delta x)}{DT_g + 39.17 T_g \Delta x} \right)$$

$$= \lim_{\Delta x \to 0} \frac{(665.89 + 17D)}{(D + 39.17\Delta x)}$$

481    $$= \frac{665.89 + 17D}{D} \tag{A3}$$

482   Note that Eq. (A3) is derived assuming the high temperature limit of viscosity η_∞ is equal to 10^{-5}

483   Pa s (Angell, 1991) in the VTF equation (Eq. 3). Similar equations for the relation between *m*

484   and *D* were given by previous studies using different η_∞ and units (Angell et al., 1994; Angell,

485   2002; Bones et al., 2012) and applying those gave very similar results in our study.

486

Atmospheric
Chemistry
and Physics
Discussions

493

494   **References.**

495   Abbatt, J. P. D., Lee, A. K. Y., and Thornton, J. A.: Quantifying trace gas uptake to tropospheric
496   aerosol: recent advances and remaining challenges, Chem. Soc. Rev., 41, 6555-6581, 2012.

497   Abramson, E., Imre, D., Beranek, J., Wilson, J., and Zelenyuk, A.: Experimental determination
498   of chemical diffusion within secondary organic aerosol particles, Physical Chemistry Chemical
499   Physics, 15, 2983-2991, 2013.

500   Aiken, A. C., DeCarlo, P. F., Kroll, J. H., et al.: O/C and OM/OC Ratios of Primary, Secondary,
501   and Ambient Organic Aerosols with High-Resolution Time-of-Flight Aerosol Mass
502   Spectrometry, Environ. Sci. Technol., 42, 4478-4485, 2008.

503   Angell, C.: Relaxation in liquids, polymers and plastic crystals—strong/fragile patterns and
504   problems, Journal of Non-Crystalline Solids, 131, 13-31, 1991.

505   Angell, C. A., Bressel, R. D., Green, J. L., Kanno, H., Oguni, M., and Sare, E. J.: Liquid fragility
506   and the glass transition in water and aqueous solutions, Journal of Food Engineering, 22, 115-
507   142, 1994.

508   Angell, C. A.: Formation of glasses from liquids and biopolymers, Science, 267, 1924-1935,
509   1995.

510   Angell, C. A.: Entropy and fragility in supercooling liquids, National Institute of Standards and
511   Technology, Journal of Research, 102, 171-185, 1997.

512   Angell, C. A.: Liquid Fragility and the Glass Transition in Water and Aqueous Solutions, Chem.
513   Rev., 102, 2627-2650, 2002.

514   Arangio, A. M., Slade, J. H., Berkemeier, T., Pöschl, U., Knopf, D. A., and Shiraiwa, M.:
515   Multiphase Chemical Kinetics of OH Radical Uptake by Molecular Organic Markers of Biomass
516   Burning Aerosols: Humidity and Temperature Dependence, Surface Reaction and Bulk
517   Diffusion, J. Phys. Chem. A, 119, 4533–4544, 2015.

Atmospheric
Chemistry
and Physics
Discussions

518   Bateman, A. P., Laskin, J., Laskin, A., and Nizkorodov, S. A.: Applications of High-Resolution
519   Electrospray Ionization Mass Spectrometry to Measurements of Average Oxygen to Carbon
520   Ratios in Secondary Organic Aerosols, Environ. Sci. Technol., 46, 8315-8324, 2012.

521   Bateman, A. P., Bertram, A. K., and Martin, S. T.: Hygroscopic Influence on the Semisolid-to-
522   Liquid Transition of Secondary Organic Materials, J. Phys. Chem. A, 119, 4386-4395, 2015.

523   Bateman, A. P., Gong, Z., Liu, P., et al.: Sub-micrometre particulate matter is primarily in liquid
524   form over Amazon rainforest, Nat. Geosci., 9, 34-37, 2016.

525   Baustian, K. J., Wise, M. E., Jensen, E. J., Schill, G. P., Freedman, M. A., and Tolbert, M. A.:
526   State transformations and ice nucleation in amorphous (semi-)solid organic aerosol, Atmos.
527   Chem. Phys., 13, 5615-5628, 2013.

528   Berkemeier, T., Shiraiwa, M., Pöschl, U., and Koop, T.: Competition between water uptake and
529   ice nucleation by glassy organic aerosol particles, Atmos. Chem. Phys., 14, 12513-12531, 2014.

530   Berkemeier, T., Steimer, S., Krieger, U. K., Peter, T., Poschl, U., Ammann, M., and Shiraiwa,
531   M.: Ozone uptake on glassy, semi-solid and liquid organic matter and the role of reactive oxygen
532   intermediates in atmospheric aerosol chemistry, Phys. Chem. Chem. Phys., 18, 12662-12674,
533   2016.

534   Boehmer, R., Ngai, K. L., Angell, C. A., and Plazek, D. J.: Nonexponential relaxations in strong
535   and fragile glass formers, J. Chem. Phys., 99, 4201-4209, 1993.

536   Bones, D. L., Reid, J. P., Lienhard, D. M., and Krieger, U. K.: Comparing the mechanism of
537   water condensation and evaporation in glassy aerosol, Proc. Natl. Acad. Sci. U.S.A., 109, 11613-
538   11618, 2012.

539   Booth, A. M., Murphy, B., Riipinen, I., Percival, C. J., and Topping, D. O.: Connecting Bulk
540   Viscosity Measurements to Kinetic Limitations on Attaining Equilibrium for a Model Aerosol
541   Composition, Environ. Sci. Technol., 48, 9298-9305, 2014.

542   Cappa, C. D., and Wilson, K. R.: Evolution of organic aerosol mass spectra upon heating:
543   implications for OA phase and partitioning behavior, Atmos. Chem. Phys., 11, 1895-1911, 2011.

544   Cappa, C. D., and Wilson, K. R.: Multi-generation gas-phase oxidation, equilibrium partitioning,
545   and the formation and evolution of secondary organic aerosol, Atmos. Chem. Phys., 12, 9505-
546   9528, 2012.

547   Chen, Q., Liu, Y., Donahue, N. M., Shilling, J. E., and Martin, S. T.: Particle-Phase Chemistry of
548   Secondary Organic Material: Modeled Compared to Measured O:C and H:C Elemental Ratios
549   Provide Constraints, Environ. Sci. Technol., 45, 4763–4770, 2011.

550   Davies, J. F., and Wilson, K. R.: Nanoscale interfacial gradients formed by the reactive uptake of
551   OH radicals onto viscous aerosol surfaces, Chem. Sci., 6, 7020-7027, 2015.

552   Dette, H. P., Qi, M., Schröder, D. C., Godt, A., and Koop, T.: Glass-forming properties of 3-
553   Methylbutane-1,2,3-tricarboxylic acid and its mixtures with water and pinonic acid, J. Phys.
554   Chem. A, 118, 7024-7033, 2014.

555   Dette, H. P., and Koop, T.: Glass Formation Processes in Mixed Inorganic/Organic Aerosol
556   Particles, J. Phys. Chem. A, 119, 4552-4561, 2015.

557   Donahue, N. M., Robinson, A. L., Stanier, C. O., and Pandis, S. N.: Coupled partitioning,
558   dilution, and chemical aging of semivolatile organics, Environ. Sci. Technol., 40, 2635-2643,
559   2006.

560   Donahue, N. M., Epstein, S. A., Pandis, S. N., and Robinson, A. L.: A two-dimensional volatility
561   basis set: 1. organic-aerosol mixing thermodynamics, Atmos. Chem. Phys., 11, 3303-3318, 2011.

562   Fox Jr, T. G., and Flory, P. J.: Second‐order transition temperatures and related properties of
563   polystyrene. I. Influence of molecular weight, J. Appl. Phys., 21, 581-591, 1950.

564   Gao, S., Ng, N. L., Keywood, M., et al.: Particle phase acidity and oligomer formation in
565   secondary organic aerosol, Environ. Sci. Technol., 38, 6582-6589, 2004.

566   Goldstein, A. H., and Galbally, I. E.: Known and unexplored organic constituents in the earth's
567   atmosphere, Environ. Sci. Technol., 41, 1514-1521, 2007.

568   Grayson, J. W., Zhang, Y., Mutzel, A., Renbaum-Wolff, L., Böge, O., Kamal, S., Herrmann, H.,
569   Martin, S. T., and Bertram, A. K.: Effect of varying experimental conditions on the viscosity of
570   α-pinene derived secondary organic material, Atmos. Chem. Phys., 16, 6027-6040, 2016.

571   Grayson, J. W., Evoy, E., Song, M., et al.: The effect of hydroxyl functional groups and molar
572   mass on the viscosity of non-crystalline organic and organic–water particles, Atmos. Chem.
573   Phys., 17, 8509-8524, 2017.

574   Gunthe, S. S., King, S. M., Rose, D., et al.: Cloud condensation nuclei in pristine tropical
575   rainforest air of Amazonia: size-resolved measurements and modeling of atmospheric aerosol
576   composition and CCN activity, Atmos. Chem. Phys., 9, 7551-7575, 2009.

577   Hancock, B. C., and Zografi, G.: The relationship between the glass transition temperature and
578   the water content of amorphous pharmaceutical solids, Pharm. Res., 11, 471-477, 1994.

579   Hildebrandt Ruiz, L., Paciga, A. L., Cerully, K. M., Nenes, A., Donahue, N. M., and Pandis, S.
580   N.: Formation and aging of secondary organic aerosol from toluene: changes in chemical
581   composition, volatility, and hygroscopicity, Atmos. Chem. Phys., 15, 8301-8313, 2015.

582   Hinks, M. L., Brady, M. V., Lignell, H., et al.: Effect of viscosity on photodegradation rates in
583   complex secondary organic aerosol materials, Phys. Chem. Chem. Phys., 18, 8785-8793, 2016.

584   Hinks, M. L., Montoya-Aguilera, J., Ellison, L., Lin, P., Laskin, A., Laskin, J., Shiraiwa, M.,
585   Dabdub, D., and Nizkorodov, S. A.: Effect of Relative Humidity on the Composition of

586   Secondary Organic Aerosol from Oxidation of Toluene, Atmos. Chem. Phys. Discuss., 2017, 1-
587   16, 2017.

588   Hosny, N. A., Fitzgerald, C., Vysniauskas, A., et al.: Direct imaging of changes in aerosol
589   particle viscosity upon hydration and chemical aging, Chem. Sci., 7, 1357-1367, 2016.

590   Huang, D., and McKenna, G. B.: New insights into the fragility dilemma in liquids, J. Chem.
591   Phys., 114, 5621-5630, 2001.

592   Ignatius, K., Kristensen, T. B., Järvinen, E., et al.: Heterogeneous ice nucleation of viscous
593   secondary organic aerosol produced from ozonolysis of α-pinene, Atmos. Chem. Phys., 16,
594   6495-6509, 2016.

595   Itoh, N., Aoyagi, Y., and Yarita, T.: Optimization of the dopant for the trace determination of
596   polycyclic aromatic hydrocarbons by liquid chromatography/dopant-assisted atmospheric-
597   pressure photoionization/mass spectrometry, J. Chromatogr. A, 1131, 285-288, 2006.

598   Jain, S., and Petrucci, G. A.: A New Method to Measure Aerosol Particle Bounce Using a
599   Cascade Electrical Low Pressure Impactor, Aerosol Sci. Technol., 49, 390-399, 2015.

600   Jathar, S. H., Cappa, C. D., Wexler, A. S., Seinfeld, J. H., and Kleeman, M. J.: Multi-
601   generational oxidation model to simulate secondary organic aerosol in a 3-D air quality model,
602   Geosci. Model Dev., 8, 2553-2567, 2015.

603   Jimenez, J. L., Canagaratna, M. R., Donahue, N. M., et al.: Evolution of organic aerosols in the
604   atmosphere, Science, 326, 1525-1529, 2009.

605   Kidd, C., Perraud, V., Wingen, L. M., and Finlayson-Pitts, B. J.: Integrating phase and
606   composition of secondary organic aerosol from the ozonolysis of alpha-pinene, Proc. Natl. Acad.
607   Sci. U.S.A., 111, 7552-7557, 2014.

608   Kiontke, A., Oliveira-Birkmeier, A., Opitz, A., and Birkemeyer, C.: Electrospray ionization
609   efficiency is dependent on different molecular descriptors with respect to solvent ph and
610   instrumental configuration, PLoS One, 11, e0167502/0167501-e0167502/0167516, 2016.

611   Koop, T., Bookhold, J., Shiraiwa, M., and Pöschl, U.: Glass transition and phase state of organic
612   compounds: dependency on molecular properties and implications for secondary organic
613   aerosols in the atmosphere, Phys. Chem. Chem. Phys., 13, 19238-19255, 2011.

614   Kuwata, M., and Martin, S. T.: Phase of atmospheric secondary organic material affects its
615   reactivity, Proc. Natl. Acad. Sci. U.S.A., 109, 17354-17359, 2012.

616   Kuwata, M., Zorn, S. R., and Martin, S. T.: Using elemental ratios to predict the density of
617   organic material composed of carbon, hydrogen, and oxygen, Environ. Sci. Technol., 46, 787-
618   794, 2012.

Atmospheric
Chemistry
and Physics
Discussions

619   Lambe, A. T., Ahern, A. T., Williams, L. R., et al.: Characterization of aerosol photooxidation
620   flow reactors: heterogeneous oxidation, secondary organic aerosol formation and cloud
621   condensation nuclei activity measurements, Atmos. Meas. Tech., 4, 445-461, 2011a.

622   Lambe, A. T., Onasch, T. B., Massoli, P., et al.: Laboratory studies of the chemical composition
623   and cloud condensation nuclei (CCN) activity of secondary organic aerosol (SOA) and oxidized
624   primary organic aerosol (OPOA), Atmos. Chem. Phys., 11, 8913-8928, 2011b.

625   Li, Y., Pöschl, U., and Shiraiwa, M.: Molecular corridors and parameterizations of volatility in
626   the chemical evolution of organic aerosols, Atmos. Chem. Phys., 16, 3327-3344, 2016.

627   Li, Y. J., Liu, P., Gong, Z., Wang, Y., Bateman, A. P., Bergoend, C., Bertram, A. K., and Martin,
628   S. T.: Chemical Reactivity and Liquid/Nonliquid States of Secondary Organic Material, Environ.
629   Sci. Technol., 49, 13264-13274, 2015.

630   Lienhard, D. M., Huisman, A. J., Krieger, U. K., et al.: Viscous organic aerosol particles in the
631   upper troposphere: diffusivity-controlled water uptake and ice nucleation?, Atmos. Chem. Phys.,
632   15, 13599-13613, 2015.

633   Lignell, H., Hinks, M. L., and Nizkorodov, S. A.: Exploring matrix effects on photochemistry of
634   organic aerosols, Proc. Natl. Acad. Sci. U.S.A., 111, 13780-13785, 2014.

635   Liu, P., Li, Y. J., Wang, Y., Gilles, M. K., Zaveri, R. A., Bertram, A. K., and Martin, S. T.:
636   Lability of secondary organic particulate matter, Proc. Natl. Acad. Sci. U.S.A., 113, 12643-
637   12648, 2016.

638   Maclean, A. M., Butenhoff, C. L., Grayson, J. W., Barsanti, K., Jimenez, J. L., and Bertram, A.
639   K.: Mixing times of organic molecules within secondary organic aerosol particles: a global
640   planetary boundary layer perspective, Atmos. Chem. Phys., 17, 13037-13048, 2017.

641   Marshall, F. H., Miles, R. E. H., Song, Y.-C., Ohm, P. B., Power, R. M., Reid, J. P., and Dutcher,
642   C. S.: Diffusion and reactivity in ultraviscous aerosol and the correlation with particle viscosity,
643   Chem. Sci., 7, 1298-1308, 2016.

644   Matsushima, S., Takano, A., Takahashi, Y., and Matsushita, Y.: Precise synthesis of a series of
645   poly(4-n-alkylstyrene)s and their glass transition temperatures, Journal of Polymer Science Part
646   B: Polymer Physics, 55, 757-763, 2017.

647   Mikhailov, E., Vlasenko, S., Martin, S. T., Koop, T., and Pöschl, U.: Amorphous and crystalline
648   aerosol particles interacting with water vapor: conceptual framework and experimental evidence
649   for restructuring, phase transitions and kinetic limitations, Atmos. Chem. Phys., 9, 9491-9522,
650   2009.

651   Montserrat, S., and Colomer, P.: The effect of the molecular weight on the glass transition
652   temperature in amorphous poly(ethylene terephthalate), Polymer Bulletin, 12, 173-180, 1984.

653   Murray, B. J., Wilson, T. W., Dobbie, S., et al.: Heterogeneous nucleation of ice particles on
654   glassy aerosols under cirrus conditions, Nat. Geosci., 3, 233-237, 2010.

Atmospheric
Chemistry
and Physics
Discussions

655   Nakanishi, M., and Nozaki, R.: Systematic study of the glass transition in polyhydric alcohols,
656   Physical Review E, 83, 051503, 2011.

657   Nguyen, T. B., Nizkorodov, S. A., Laskin, A., and Laskin, J.: An approach toward quantification
658   of organic compounds in complex environmental samples using high-resolution electrospray
659   ionization mass spectrometry, Anal. Methods, 5, 72-80, 2013.

660   Nizkorodov, S. A., Laskin, J., and Laskin, A.: Molecular chemistry of organic aerosols through
661   the application of high resolution mass spectrometry, Phys. Chem. Chem. Phys., 13, 3612-3629,
662   2011.

663   Nozière, B., Kalberer, M., Claeys, M., et al.: The Molecular Identification of Organic
664   Compounds in the Atmosphere: State of the Art and Challenges, Chem. Rev., 115, 3919–3983,
665   2015.

666   O'Connell, P. A., and McKenna, G. B.: Arrhenius-type temperature dependence of the segmental
667   relaxation below T g, J. Chem. Phys., 110, 11054-11060, 1999.

668   Onder, K., Peters, R. H., and Spark, L. C.: Melting and transition phenomena in some polyester-
669   urethanes, Polymer, 13, 133-139, 1972.

670   Pajunoja, A., Malila, J., Hao, L., Joutsensaari, J., Lehtinen, K. E. J., and Virtanen, A.: Estimating
671   the viscosity range of SOA particles based on their coalescence time, Aerosol Sci. Technol., 48,
672   i-iv, 2014.

673   Pajunoja, A., Lambe, A. T., Hakala, J., et al.: Adsorptive uptake of water by semisolid secondary
674   organic aerosols, Geophys. Res. Lett., 42, 3063-3068, 2015.

675   Papadopoulos, P., Floudas, G., Chi, C., and Wegner, G.: Molecular dynamics of oligofluorenes:
676   A dielectric spectroscopy investigation, J. Chem. Phys., 120, 2368-2374, 2004.

677   Perraud, V., Bruns, E. A., Ezell, M. J., et al.: Nonequilibrium atmospheric secondary organic
678   aerosol formation and growth, Proc. Natl. Acad. Sci. U.S.A., 109, 2836-2841, 2012.

679   Petters, M. D., and Kreidenweis, S. M.: A single parameter representation of hygroscopic growth
680   and cloud condensation nucleus activity, Atmos. Chem. Phys., 7, 1961-1971, 2007.

681   Petters, S. S., Pagonis, D., Claflin, M. S., Levin, E. J. T., Petters, M. D., Ziemann, P. J., and
682   Kreidenweis, S. M.: Hygroscopicity of Organic Compounds as a Function of Carbon Chain
683   Length and Carboxyl, Hydroperoxy, and Carbonyl Functional Groups, J. Phys. Chem. A, 121,
684   5164-5174, 2017.

685   Polymer handbook, t. e.: J. Brandrup (Editor), Edmund H. Immergut (Editor), E. A. Grulke
686   (Editor), John Wiley & Sons, Inc., ISBN 0-471-16628-6, 1999.

687   Price, H. C., Murray, B. J., Mattsson, J., O'Sullivan, D., Wilson, T. W., Baustian, K. J., and
688   Benning, L. G.: Quantifying water diffusion in high-viscosity and glassy aqueous solutions using
689   a Raman isotope tracer method, Atmos. Chem. Phys., 14, 3817-3830, 2014.

690   Putman, A. L., Offenberg, J. H., Fisseha, R., Kundu, S., Rahn, T. A., and Mazzoleni, L. R.:
691   Ultrahigh-resolution FT-ICR mass spectrometry characterization of α-pinene ozonolysis SOA,
692   Atmos. Environ., 46, 164-172, 2012.

693   Raffaelli, A., and Saba, A.: Atmospheric pressure photoionization mass spectrometry, Mass
694   Spectrom. Rev., 22, 318-331, 2003.

695   Renbaum-Wolff, L., Grayson, J. W., Bateman, A. P., Kuwata, K., Sellier, M., Murray, B. J.,
696   Schilling, J. E., Martin, S. T., and Bertram, A. K.: Viscosity of α-pinene secondary organic
697   material and implications for particle growth and reactivity, Proc. Natl. Acad. Sci. U.S.A., 110,
698   8014-8019, 2013.

699   Roach, P. J., Laskin, J., and Laskin, A.: Nanospray desorption electrospray ionization: an
700   ambient method for liquid-extraction surface sampling in mass spectrometry, Analyst
701   (Cambridge, U. K.), 135, 2233-2236, 2010a.

702   Roach, P. J., Laskin, J., and Laskin, A.: Molecular Characterization of Organic Aerosols Using
703   Nanospray-Desorption/Electrospray Ionization-Mass Spectrometry, Anal. Chem. (Washington,
704   DC, U. S.), 82, 7979-7986, 2010b.

705   Roos, Y.: Melting and glass transitions of low molecular weight carbohydrates, Carbohydr. Res.,
706   238, 39-48, 1993.

707   Rothfuss, N. E., and Petters, M. D.: Influence of Functional Groups on the Viscosity of Organic
708   Aerosol, Environ. Sci. Technol., 51, 271-279, 2017.

709   Saukko, E., Lambe, A. T., Massoli, P., et al.: Humidity-dependent phase state of SOA particles
710   from biogenic and anthropogenic precursors, Atmos. Chem. Phys., 12, 7517-7529, 2012.

711   Schill, G. P., and Tolbert, M. A.: Heterogeneous ice nucleation on phase-separated organic-
712   sulfate particles: effect of liquid vs. glassy coatings, Atmos. Chem. Phys., 13, 4681-4695, 2013.

713   Schill, G. P., De Haan, D. O., and Tolbert, M. A.: Heterogeneous Ice Nucleation on Simulated
714   Secondary Organic Aerosol, Environ. Sci. Technol., 48, 1675-1682, 2014.

715   Selimovic, V., Yokelson, R. J., Warneke, C., Roberts, J. M., de Gouw, J., Reardon, J., and
716   Griffith, D. W. T.: Aerosol optical properties and trace gas emissions by PAX and OP-FTIR for
717   laboratory-simulated western US wildfires during FIREX, Atmos. Chem. Phys. Discuss., 2017,
718   1-34, 2017.

719   Shiraiwa, M., Ammann, M., Koop, T., and Pöschl, U.: Gas uptake and chemical aging of
720   semisolid organic aerosol particles, Proc. Natl. Acad. Sci. U.S.A., 108, 11003-11008, 2011.

721   Shiraiwa, M., and Seinfeld, J. H.: Equilibration timescale of atmospheric secondary organic
722   aerosol partitioning, Geophys. Res. Lett., 39, L24801, 2012.

Atmospheric
Chemistry
and Physics
Discussions

723 Shiraiwa, M., Zuend, A., Bertram, A. K., and Seinfeld, J. H.: Gas-particle partitioning of
724 atmospheric aerosols: interplay of physical state, non-ideal mixing and morphology, Phys.
725 Chem. Chem. Phys., 15, 11441-11453, 2013.

726 Shiraiwa, M., Berkemeier, T., Schilling-Fahnestock, K. A., Seinfeld, J. H., and Pöschl, U.:
727 Molecular corridors and kinetic regimes in the multiphase chemical evolution of secondary
728 organic aerosol, Atmos. Chem. Phys., 14, 8323-8341, 2014.

729 Shiraiwa, M., Li, Y., Tsimpidi, A. P., Karydis, V. A., Berkemeier, T., Pandis, S. N., Lelieveld, J.,
730 Koop, T., and Pöschl, U.: Global distribution of particle phase state in atmospheric secondary
731 organic aerosols, Nat. Commun., 8, 15002, 2017.

732 Shrivastava, M., Cappa, C. D., Fan, J., et al.: Recent advances in understanding secondary
733 organic aerosol: Implications for global climate forcing, Rev. Geophys., 55, 509-559, 2017.

734 Slade, J. H., and Knopf, D. A.: Multiphase OH Oxidation Kinetics of Organic Aerosol: The Role
735 of Particle Phase State and Relative Humidity, Geophys. Res. Lett., 2014GL060582, 2014.

736 Song, M., Liu, P. F., Hanna, S. J., Li, Y. J., Martin, S. T., and Bertram, A. K.: Relative humidity-
737 dependent viscosities of isoprene-derived secondary organic material and atmospheric
738 implications for isoprene-dominant forests, Atmos. Chem. Phys., 15, 5145-5159, 2015.

739 Song, M., Liu, P. F., Hanna, S. J., Zaveri, R. A., Potter, K., You, Y., Martin, S. T., and Bertram,
740 A. K.: Relative humidity-dependent viscosity of secondary organic material from toluene photo-
741 oxidation and possible implications for organic particulate matter over megacities, Atmos. Chem.
742 Phys., 16, 8817-8830, 2016a.

743 Song, Y. C., Haddrell, A. E., Bzdek, B. R., Reid, J. P., Bannan, T., Topping, D. O., Percival, C.,
744 and Cai, C.: Measurements and Predictions of Binary Component Aerosol Particle Viscosity, J.
745 Phys. Chem. A, 120, 8123-8137, 2016b.

746 Tolocka, M. P., Jang, M., Ginter, J. M., Cox, F. J., Kamens, R. M., and Johnston, M. V.:
747 Formation of oligomers in secondary organic aerosol, Environ. Sci. Technol., 38, 1428-1434,
748 2004.

749 US-EPA: Estimation programs interface suite for microsoft windows, 2012.

750 Vaden, T. D., Imre, D., Beranek, J., Shrivastava, M., and Zelenyuk, A.: Evaporation kinetics and
751 phase of laboratory and ambient secondary organic aerosol, Proc. Natl. Acad. Sci. U.S.A., 108,
752 2190-2195, 2011.

753 van der Sman, R. G. M.: Predictions of Glass Transition Temperature for Hydrogen Bonding
754 Biomaterials, J. Phys. Chem. B, 117, 16303-16313, 2013.

755 Virtanen, A., Joutsensaari, J., Koop, T., et al.: An amorphous solid state of biogenic secondary
756 organic aerosol particles, Nature, 467, 824-827, 2010.

Atmospheric
Chemistry
and Physics
Discussions

Open Access

EGU

757   Wang, B., O'Brien, R. E., Kelly, S. T., Shilling, J. E., Moffet, R. C., Gilles, M. K., and Laskin,
758   A.: Reactivity of Liquid and Semisolid Secondary Organic Carbon with Chloride and Nitrate in
759   Atmospheric Aerosols, J. Phys. Chem. A, 119, 4498-4508, 2015.

760   Wang, B. B., Lambe, A. T., Massoli, P., Onasch, T. B., Davidovits, P., Worsnop, D. R., and
761   Knopf, D. A.: The deposition ice nucleation and immersion freezing potential of amorphous
762   secondary organic aerosol: Pathways for ice and mixed-phase cloud formation, J. Geophys. Res.-
763   Atmos., 117, D16209, 2012.

764   Williams, M. L., Landel, R. F., and Ferry, J. D.: The temperature dependence of relaxation
765   mechanisms in amorphous polymers and other glass-forming liquids, J. Am. Chem. Soc., 77,
766   3701-3707, 1955.

767   Yli-Juuti, T., Pajunoja, A., Tikkanen, O.-P., et al.: Factors controlling the evaporation of
768   secondary organic aerosol from α-pinene ozonolysis, Geophys. Res. Lett., 44, 2562-2570, 2017.

769   Zaveri, R. A., Easter, R. C., Shilling, J. E., and Seinfeld, J. H.: Modeling kinetic partitioning of
770   secondary organic aerosol and size distribution dynamics: representing effects of volatility, phase
771   state, and particle-phase reaction, Atmos. Chem. Phys., 14, 5153-5181, 2014.

772   Zhang, Y., Sanchez, M. S., Douet, C., et al.: Changing shapes and implied viscosities of
773   suspended submicron particles, Atmos. Chem. Phys., 15, 7819-7829, 2015.

774   Zhou, S., Shiraiwa, M., McWhinney, R., Pöschl, U., and Abbatt, J. P. D.: Kinetic limitations in
775   gas-particle reactions arising from slow diffusion in secondary organic aerosol, Faraday Discuss.,
776   165, 391-406, 2013.

777   Zobrist, B., Marcolli, C., Pedernera, D. A., and Koop, T.: Do atmospheric aerosols form
778   glasses?, Atmos. Chem. Phys., 8, 5221-5244, 2008.

779   Zobrist, B., Soonsin, V., Luo, B. P., Krieger, U. K., Marcolli, C., Peter, T., and Koop, T.: Ultra-
780   slow water diffusion in aqueous sucrose glasses, Phys. Chem. Chem. Phys., 13, 3514-3526,
781   2011.
782
783

784 **Table 1.** Composition classes and the n_C^0 and b values (K) for glass transition temperature

785 parameterizations obtained by least-squares optimization using the measurements compiled in

786 Koop et al., (2011), Dette et al., (2014 and Rothfuss and Petters (2017).

Classes	n_C^0	b_C	b_H	b_{CH}	b_O	b_{CO}
CH	1.96	61.99	−113.33	28.74		
	(±1.81)	(±53.65)	(±44.47)	(±20.86)		
CHO	12.13	10.95	−41.82	21.61	118.96	−24.38
	(±2.66)	(±13.60)	(±14.78)	(±5.30)	(±9.72)	(±4.21)

787

788

789

790 **Table 2.** Glass transition temperatures calculated using Eq. (1) and (2) for toluene SOA mixtures

791 at low relative humidity (low RH < 2%) and high relative humidity (high RH = 75%) conditions.

$T_{g,org}$ (K)	low RH	high RH
Equation (1)*	299	295
Equation (2)	313	303

792 * Compounds with $M > 450$ g mol^{-1} were excluded from the analysis.
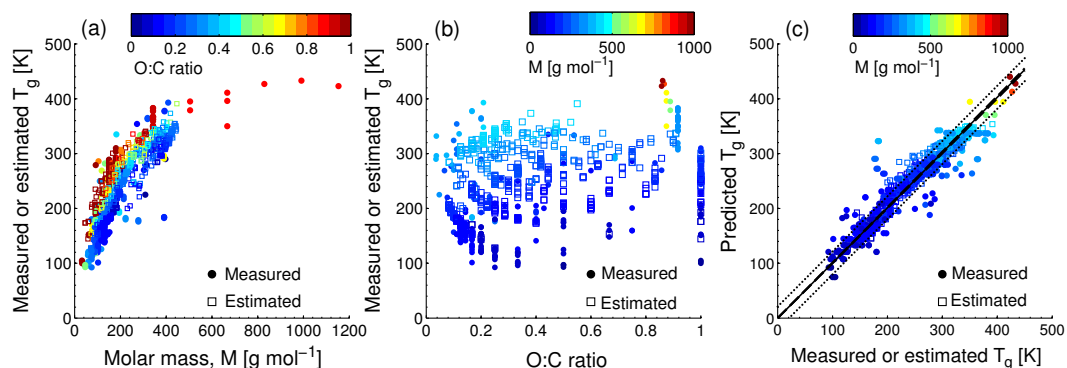
Figure 1. Characteristic relationships between molecular properties and the glass transition temperature (T_g) of organic compounds. (a) T_g of organic compounds as measured (circles) and estimated with the Boyer-Kauzmann rule (squares) plotted against molar mass. The markers are color-coded by atomic O:C ratio. (b) Measured (circles) and estimated (squares) T_g of organic compounds plotted against O:C ratio. The markers are color-coded by molar mass. (c) Predicted T_g for CHO compounds using a parameterization (Eq. 2) developed in this study compared to measured (circles) and estimated T_g by the Boyer-Kauzmann rule (squares). The solid line shows 1:1 line and the dashed and dotted lines show 68% confidence and prediction bands, respectively.
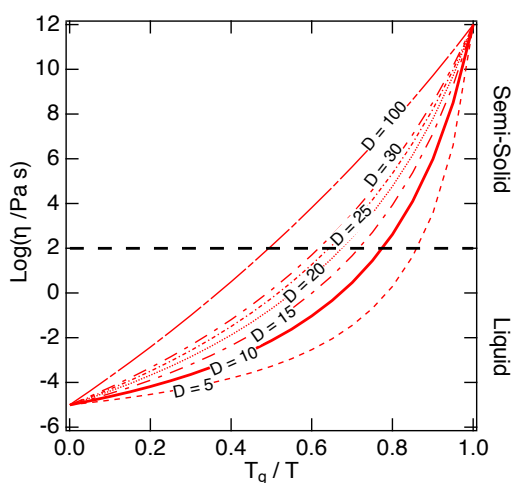
Figure 2. The Angell plot of viscosity (η) vs. T_g/T. The lines represent different fragility parameter (D) values in the range of 5 - 100, with $D = 10$ (the solid line) used as a base case for this study. A large fragility parameter value is associated with a strong glass former, while fragile materials are associated with lower values. The black dashed line at viscosity of 10^2 Pa s indicates the approximate threshold between liquid and semi-solid states.

Atmospheric
Chemistry
and Physics
Discussions

Open Access
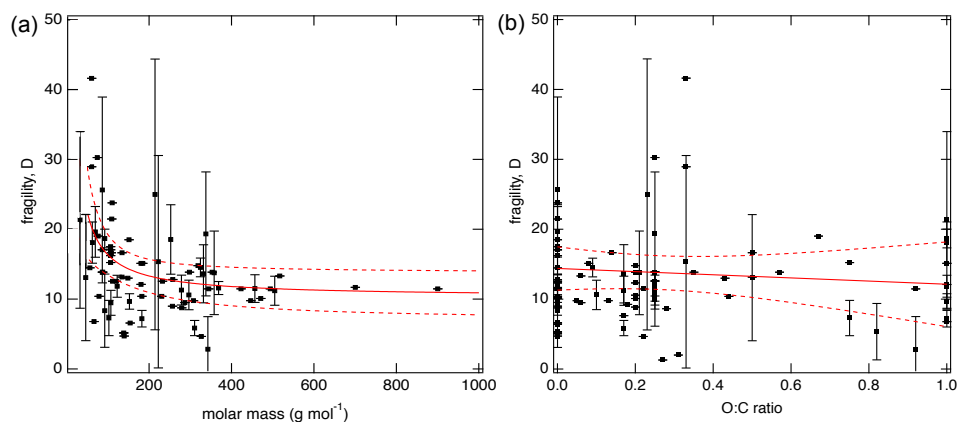
Figure 3. Fragility parameter of organic compounds (D) plotted against (a) molar mass and (b) atomic O:C ratio. Error bars are standard deviations. The solid red lines represent the fitted curves with fitted equations for (a) $D = 602.6/M + 10.3$ and (b) $D = 14.4 - 2.3(\text{O:C})$ respectively. Dashed red lines indicate the 95% confidence band.

Atmospheric
Chemistry
and Physics
Discussions
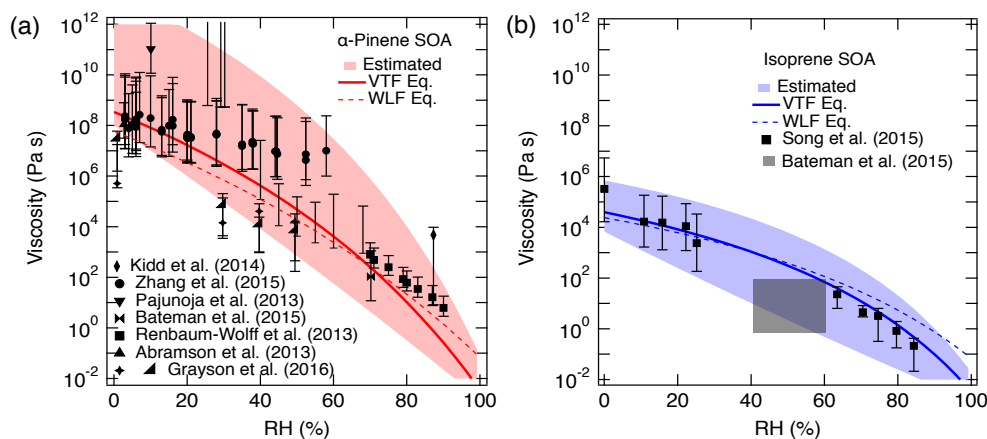
818
Figure 4. Comparison of measured and predicted viscosity of (a) α-pinene SOA and (b) isoprene
SOA at 295 K as a function of RH. The solid lines represent base simulations with the VTF
equation, while the dotted line represents viscosity predicted using the WLF equation
[parameters: glass transition temperature of dry SOA ($T_{g,org}$), fragility (D), hygroscopicity (κ)
and Gordon-Taylor constant (k_{GT})]: (a) 278.5 K, 0.1, 10 and 2.5; (b) 255 K, 0.1, 10 and 2.5. The
shaded regions were determined by varying these parameters (a) upper (lower) limit: $T_{g,org}$ = 300
K (278.5 K), κ = 0.1 (0.1), D = 20 (10), k_{GT} = 2.5 (2.0); (b) upper (lower) limit: $T_{g,org}$ = 255 K
(255 K), κ = 0.10 (0.15), D = 15 (8), k_{GT} = 2.5 (4.0). Grayson et al. (2016) data in the panel (a)
represents two different mass loadings (121 μg m^{-3}; 520 μg m^{-3}). The gray box in panel (b)
represents estimated viscosity based on bounce measurements of Bateman et al. (2015).

829
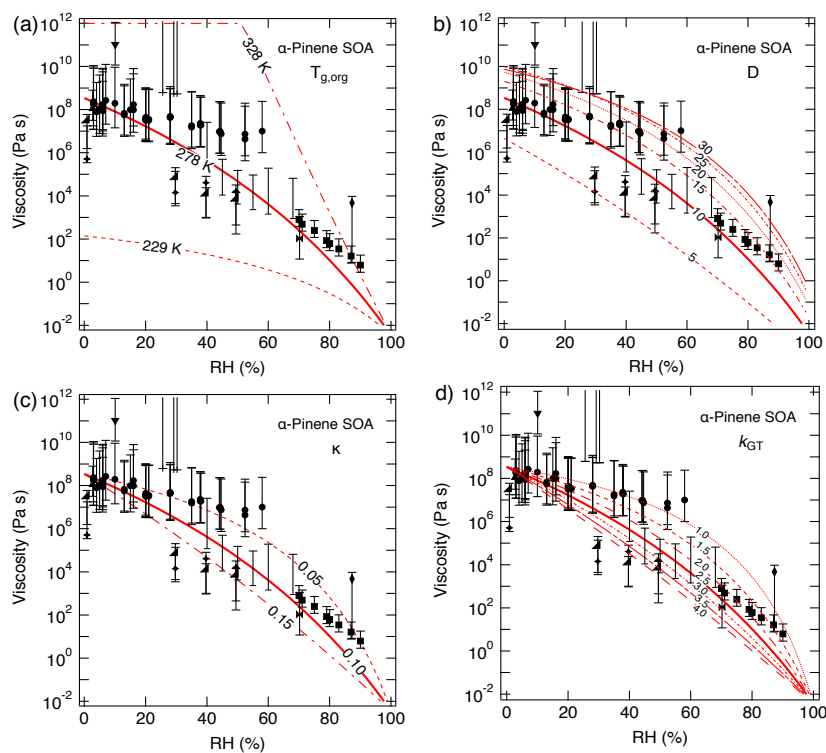
Figure 5. Sensitivity calculations for viscosity of α-pinene SOA at 295 K as a function of RH by varying: (a) glass transition temperature of dry SOA ($T_{g,org}$), (b) fragility (D), (c) hygroscopicity (κ), and (d) Gordon-Taylor constant (k_{GT}).
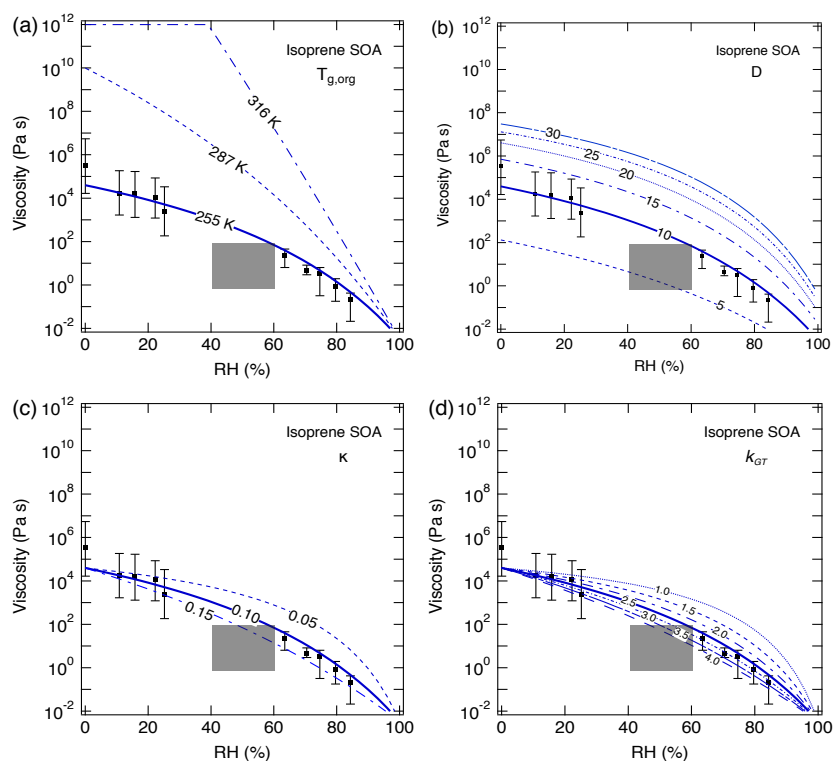
835
836
837 **Figure 6.** Sensitivity calculations for viscosity of isoprene SOA at 295 K as a function of RH by
838 varying: (a) glass transition temperature of dry SOA ($T_{g,org}$), (b) fragility (D), (c) hygroscopicity
839 (κ), and (d) Gordon-Taylor constant (k_{GT}). Data points are measured viscosity by Song et al.
840 (2015) and the gray box represents estimated viscosity based on bounce measurements of
841 Bateman et al. (2015).
842

843

Figure 7. (a) Molecular corridor of molar mass plotted against volatility of toluene SOA formed under dry conditions (Hinks et al., 2017) color-coded by glass transition temperature (T_g) estimated using Eq. (2). The upper dashed line indicates the low O:C bound of the molecular corridor (linear alkanes C_nH_{2n+2} with O:C = 0), and the lower dotted line indicates the high O:C bound (sugar alcohols $C_nH_{2n+2}O_n$ with O:C = 1). (b) Comparison of measured (markers) and modeled (lines) viscosity of toluene SOA at 295 K as a function of RH. Viscosities were calculated using fragility (D) of 13, the hygroscopicity (κ) of 0.25 and the Gordon-Taylor constant (k_{GT}) of 3.0 with different glass transition temperatures of dry SOA ($T_{g,org}$) as estimated using Eq. (1) or (2) under low and high RH conditions. The shaded regions were calculated by varying those parameters: $T_{g,org}$ = 313 K (295 K), κ = 0.20 (0.25), D = 13 (10), k_{GT} = 2.5 (3.5) for the upper (lower) limit.

855
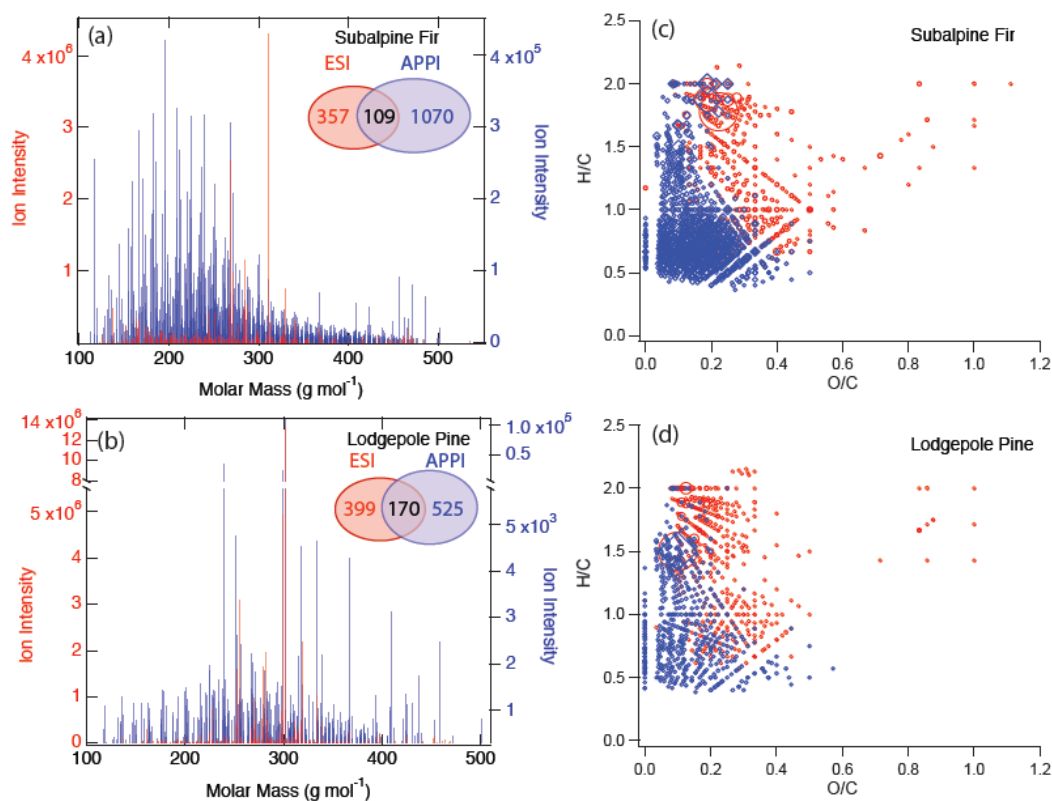
Figure 8. Mass spectra of biomass burning organic particles collected from test burns of (a) subalpine fir and (b) lodgepole pine as measured by high resolution mass spectrometry with two ionization techniques: electron spray ionization (ESI, red) and atmospheric pressure photoionization (APPI; blue). Numbers of elemental formulas identified by ESI (red), APPI (blue) and both modes (black) are also specified. Van Krevelen plots of the compounds identified by ESI (red) and APPI (blue) mode in BBOA from burning of (c) subalpine fir and (d) lodgepole pine.
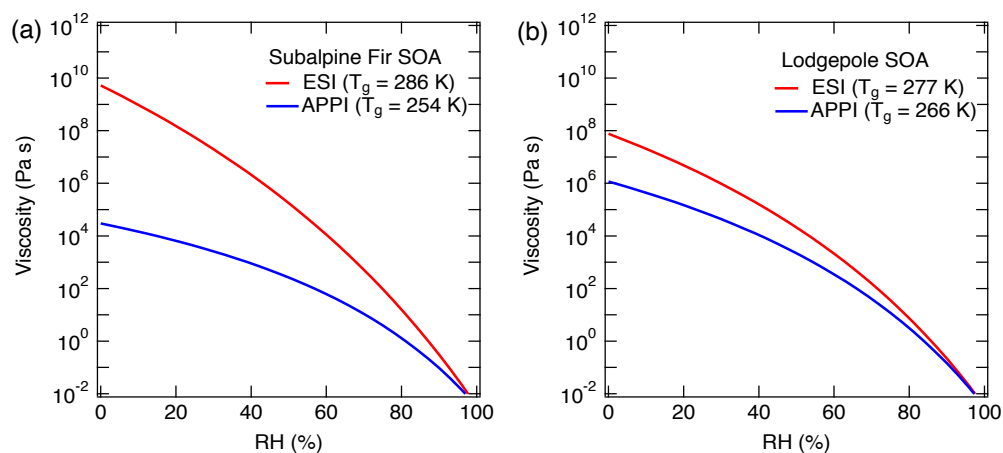
Figure 9. Predicted viscosity for biomass burning particles of (a) subalpine fir and (b) lodgepole pine trees as measured by high resolution mass spectrometry with two ionization techniques: electrospray ionization (ESI, red) and atmospheric pressure photoionization (APPI; blue). $T_{g,org}$ are specified in the figure legend and other used parameters are fixed to $\kappa = 0.1$, $D = 10$, $k_{GT} = 2.5$.
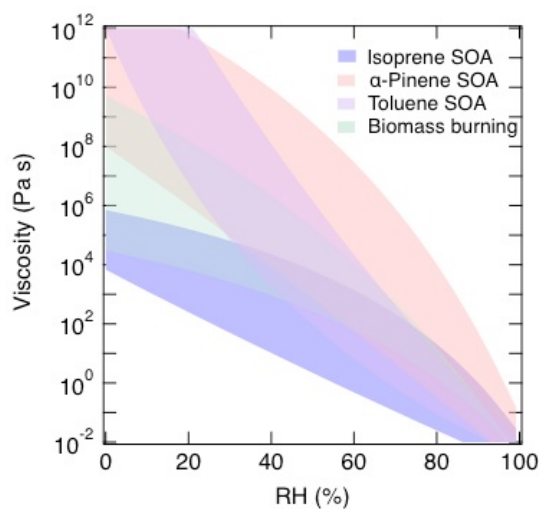

Figure 10. Summary of predicted range of viscosity of α-pinene SOA (red), isoprene SOA (blue), toluene SOA (purple), and biomass burning particles (green).
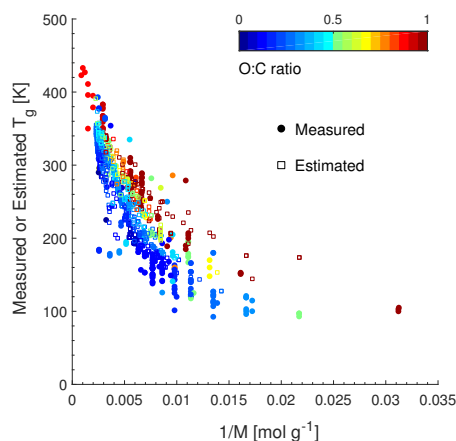
879
880 **Figure A1.** T_g of organic compounds as measured (circles) and estimated with the Boyer-
881 Kauzmann rule (squares) plotted against the inverse molar mass. The markers are color-coded by
882 atomic O:C ratio.

883

884
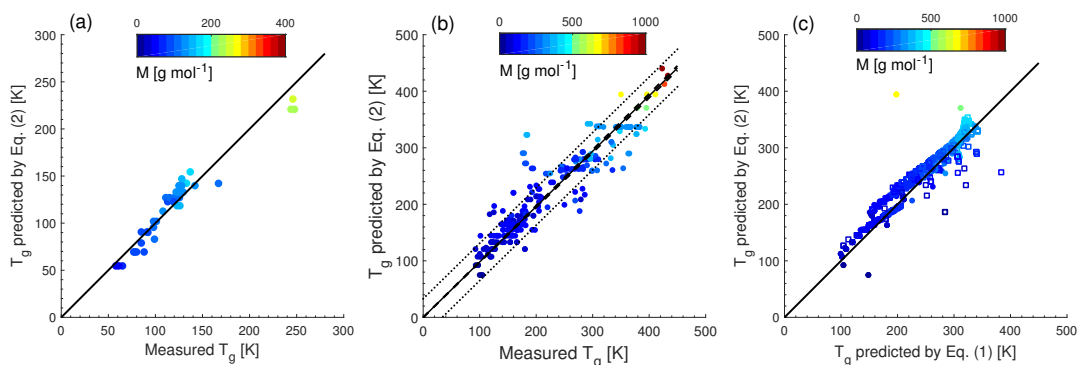
885

886 **Figure A2.** Predicted T_g using Eq. (2) compared with (a) measured T_g for (a) CH and (b) CHO
887 compounds and (c) predicted T_g using Eq. (1) for CHO compounds. The solid line shows 1:1 line
888 and the dashed and dotted lines in the panel (c) show 68% confidence and prediction bands,
889 respectively. In panel (c), solid circle markers represent measured T_g and open square markers
890 represent estimated T_g by the Boyer-Kauzmann rule.